

Feasibility of Measuring Fast Neutron Background Using Muon Detectors

Jianglai Liu
Caltech

January 3, 2007

Abstract

In this note, I combine the RPC and the water pool muon systems, and study their efficiency for tagging the fast neutron background.

1 Introduction

In [1], Laur Littenberg pointed out that the key purpose of the muon detector is not to measure muons, but rather to veto the muon-induced fast neutron background. The fast neutrons can be sorted into two types according to the nature of their parent muons: a) those that should have been “tagged”, but missed by both muon systems due to their inefficiencies; b) those that *cannot* be tagged. For a), Laur discussed a standard method to determine the residual neutron background, under the assumption that the inefficiency of the two muon systems are uncorrelated. For b), Laur proposed a method, which use a scaling to the tagged fast neutron prompt energy spectrum, with an assumption that the tagged and untagged fast neutrons have very similar energy spectrum. Bob McKeown pointed out in [2] that RPC-tagged fast neutrons may provide additional information about the untagged background, which should allow us to validate/tune our Monte Carlo to *calculate* of the untagged background. The rest of note is organized to scrutinize these thoughts with simulation. In Sec. 2, we report a simulation with both RPC and water pool as the muon detectors, and examine the nature of their inefficiencies. In Sec. 3, we describe the mechanics of the muon-induced spallation neutron simulation. Finally in Sec. 4, the feasibility to measure the fast neutron backgrounds using the muon system is examined.

2 Efficiency of Muon System with a “Grand Water Pool” and RPC

A single Čerenkov water pool as a muon detector has been studied extensively, e.g. in [3]. In this study, a small variation is made to the baseline configuration of the water pool, namely, the 1 m thick water modules outside the pool is removed, and the size of the pool is expanded in each direction by 1 m accordingly. This is the so-called “grand water pool” configuration. Only one layer of 8” PMTs (facing inward) is implemented at the pool surface (*except the top*), with a density of 2 m² per tube. For the near halls, the “grand” pool now have a dimension of 16 × 10 × 10 m, with 329 tubes in total. The inner pool surface is coated with a layer of tyvek with ~0.8 reflectivity to enhance the Čerenkov light collection. As a modification to previous simulations, the attenuation length of the water has been set to a more realistic ~30 m, instead of 50 m in [3]. A RPC “roof” is placed on top of the water pool. The RPC is extended into the rock, with a horizontal overlap of 1 m. The full configuration is illustrated in Fig. 1.

Data files specifying the muon energy and direction distributions at the underground halls from [4] are used to generate muons. The muons are “thrown in” from a box surface enclosing at least 1 m of rock (the outermost grayish box in Fig. 1). The choice of 1 m shall be discussed in Sec. 3. The incident point of

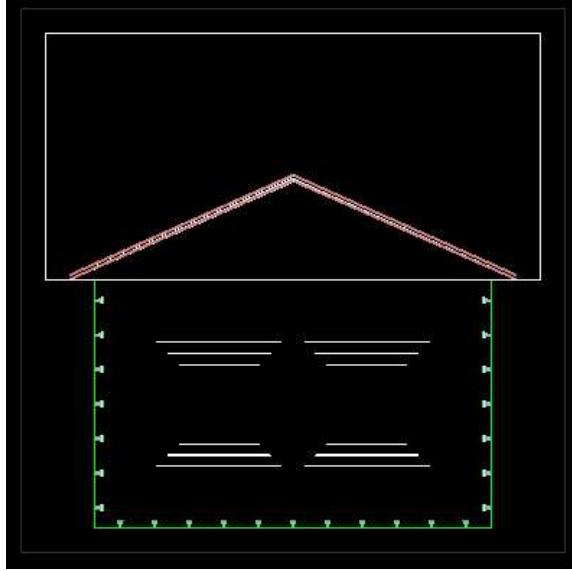


Figure 1: The “grand water pool” configuration with RPC roof in this simulation. Some PMTs are removed from the figures for visual clarity.

the muons are randomly chosen on the box surfaces in such a way to reflect the incident muon flux. In the remainder of this note, unless otherwise specified, all simulation studies are made for the Daya Bay near site, although most of the conclusions apply to other experimental halls as well.

As discussed in [3], a simple muon trigger based on the number of fired tubes is assumed in the simulation. The trigger threshold is set to be high enough such that the random veto deadtime loss is less than 1%. For a veto gate of $200 \mu\text{s}$, a single rate of 50 kHz per tube, and 329 tubes, this requirement leads to a trigger condition of $n_{\text{hits}} \geq 16$ [3].

The total number of muons (N_{tot}) is defined as those that have non-zero energy deposit (or non-zero track length) *in the water*. To study the combined muon efficiency with the RPC and pool systems, we divide these events into subsets: a) number of muons that fire at least n_{hits} number of tubes (N_{water}); b) number of muons that either fire at least n_{hits} number of tubes, or fire the RPC ($N_{\text{water||rpc}}$); and c) number of muons that fires both the water pool and the RPC ($N_{\text{water\&rpc}}$). At this stage, the RPC trigger is simply a requirement of non-zero energy deposit. Three muon efficiencies are defined

$$\epsilon_{\text{water}} = \frac{N_{\text{water}}}{N_{\text{tot}}}, \quad \epsilon_{\text{rpc}} = \frac{N_{\text{water\&rpc}}}{N_{\text{water}}}, \quad \epsilon_{\text{water||rpc}} = \frac{N_{\text{water||rpc}}}{N_{\text{tot}}}. \quad (1)$$

In addition, we calculate the efficiency of the RPC to those muons that do *not* trigger the water pool ($\tilde{\epsilon}_{\text{rpc}}$) as

$$\tilde{\epsilon}_{\text{rpc}} \equiv \frac{\epsilon_{\text{water||rpc}} - \epsilon_{\text{water}}}{1 - \epsilon_{\text{water}}}. \quad (2)$$

Obviously, $\tilde{\epsilon}_{\text{rpc}}$ will be different from ϵ_{rpc} , unless the inefficiencies of the pool and the RPC are completely *uncorrelated*. In Fig. 2, ϵ_{water} and $\epsilon_{\text{water||rpc}}$ are plotted as a function of n_{hits} threshold. At our nominal $n_{\text{hits}} = 16$, ϵ_{water} and $\epsilon_{\text{water||rpc}}$ are $99.0 \pm 0.2\%$ and $99.6 \pm 0.2\%$, respectively. For relatively small muon signals, n_{hits} as a function of the muon track length in the water is plotted in Fig. 3, and on average $n_{\text{hits}} \sim 100/\text{m}$. Therefore the water pool becomes insensitive to muons with less than 0.2 m track in the water (“corner clippers”). This is also illustrated in the 1D purple histogram in Fig. 3. ϵ_{rpc} , on the other hand, stays at 54%. The relative low efficiency of the RPC is due to the fact that it has little geometric coverage to the muons entering the side of the pool, rather than that it is inefficient to the muons that cross it. Indeed, for the 18 muons (out of 1804 in this study) with $n_{\text{hits}} \leq 16$, the 10 that enter from the top of the pool are all caught by the RPC, while all of the rest entering from the sides are missed. To further examine inefficiencies of the two muon systems, $\tilde{\epsilon}_{\text{rpc}}$ calculated from Eqn. 2 is overlaid in Fig. 2 (on a different Y

scale). The fact that it has a value close to 54% confirms that the two muon systems have uncorrelated inefficiencies.

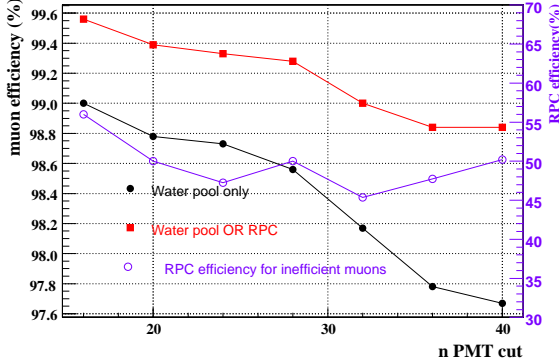


Figure 2: Muon efficiency for water pool only (black) and water pool OR RPC (red) vs. the trigger threshold on nhits (ordinate on the left, and $\bar{\epsilon}_{\text{RPC}}$ (purple) from Eqn. 2 (ordinate on the right). The statistical uncertainties for black and red data points are 0.2-0.3%, and those for the purple points are 7%-12%.

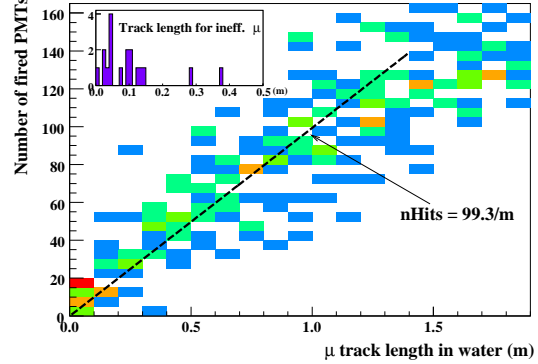


Figure 3: Number of fired PMTs in the water pool vs muon track length in water (2D) with a linear fit. The track length distribution (1D) for those muons with nhits < 16 is overlaid.

3 Simulation of Muon-induced Spallation Neutron

In this section, we shift focus to discuss the true background – the muon-induced spallation neutrons. Ideally, GEANT4 can be directly used to simulate these events [5]. However, it was realized that doing so was extremely CPU costly. Alternatively, we chose to apply the parameterization of the spallation neutron production in [6], and use the following two-step procedure to break up the neutron production and neutron transport.

First, the muon events are generated the same way as described in Sec. 2. However, the Čerenkov process was turned off to minimize CPU usage. For the neutron tagging study later in Sec. 4, we shall simply use the muon track length in water to *predict* the total nhits (Fig. 3). For spallation neutrons, instead of letting GEANT4 to simulate their production, we created neutrons by hand along the muon trajectory. Specifically, every muon track is divided into segments, each with 10 g/cm² total material thickness. At the end of each segment, a neutron is generated (*but not transported*) according to the neutron energy and $\cos\theta$ spectra in [6]. Since soft neutrons hardly make into the central detector, to speed up the simulation for the next step, we sampled the neutron energy between 100 MeV[†] and 2 GeV. The neutron production probability in liquid scintillator in [7], corrected for materials with different atomic mass as well as for the neutron energy cutoff, is assigned as the event weight to this neutron, i.e.,

$$\text{weight} = 4.14 \times 10^{-6} E_{\mu}^{0.74} / (\text{g/cm}^2) \times 10 \text{g/cm}^2 \times f_A \times f_{100\text{MeV}} \quad (3)$$

where E_{μ} is the average muon kinetic energy in GeV at this track segment. The first correction factor, $f_A = \left(\frac{A}{A_{\text{scint}}}\right)^{0.82}$, is given in [7], with A and A_{scint} being the atomic masses of the track segment material and the liquid scintillator respectively. The second correction factor, $f_{100\text{MeV}}$, is the fraction of neutrons with an energy ≥ 100 MeV. Apparently it should be increasing with the muon energy. The energy spectrum parameterization given in [6] diverges at zero neutron energy. Therefore instead of carrying out an analytical integration, we determined $f_{100\text{MeV}}$ from the GEANT4 neutron production data in [5] at various muon energies. The results are shown in Fig. 4, from which we obtained an empirical parameterization:

$$f_{100\text{MeV}} = 0.037 + 0.027 \log(E_{\mu}) - 1.8 \times 10^{-3} (\log(E_{\mu}))^2 \quad (4)$$

[†]The choice of 100 MeV is consistent with that in [8].

The typical value for the weight for a neutron, calculated from Eqn. 3, is 10^{-4} , and on average ~ 200 neutrons

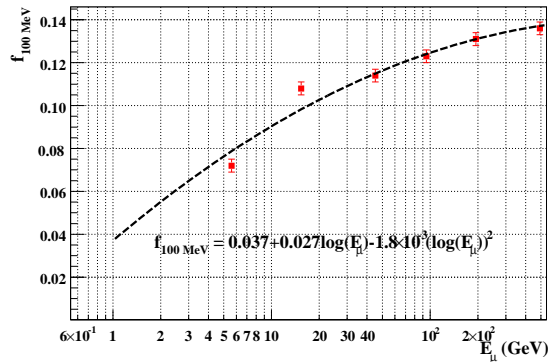


Figure 4: *The fraction of spallation neutrons produced in liquid scintillator with KE > 100 MeV at various incident muon energies. Data from [5].*

are generated along each muon track. After all these treatments, the production vertices, momenta, the event weights, as well as the parent muon track information for these neutrons are stored into a data file.

Second, the data file created in the first step are used as the neutron generator. Each neutron is transported through the water pool geometry illustrated in Fig. 1. When any neutron enters or gets produced in the Gd-loaded scintillator volume, its kinetic energy is stored in an output tree. Neutrons from the rock rarely enters the target (out of ~ 5 M neutrons generated in the first step, only ~ 100 rock neutrons makes into the target). Therefore instead of using a complicated energy/time cut to identify fast neutron background, we adopted a simple and conservative cut on the KE of the neutrons that enters the target region:

$$\text{“fast neutrons”} = \text{neutrons with an entering KE between 4 and 20 MeV}, \quad (5)$$

since on average these neutrons will deposit a visible prompt energy between ~ 0.75 MeV and 8 MeV [‡]. Events with more than one neutrons (from the same parent neutron) entering the target occur rather frequently (see Fig. 10). In this case, we sum up the KEs for these neutrons, and apply the KE cut in Eqn. 5. If passed, they are counted as one fast neutron hit (with the neutron multiplicity recorded). The total fast neutron background rate can then be calculated as

$$R_{\text{fast}} = R_\mu \frac{\sum \text{weight}}{N_\mu}, \quad (6)$$

where the “ \sum ” sums over all events identified as fast neutrons, and N_μ is the total number of muons generated in the first step. R_μ is the associating cosmic muon rate incident on the entire box enclosure, which can be estimated as

$$R_\mu = r_\mu A \left(1 + \frac{N_{\text{side}}}{N_{\text{top}}}\right), \quad (7)$$

where r_μ is the muon rate per unit area given in [4], A is the top area of the box surface, and $\frac{N_{\text{side}}}{N_{\text{top}}}$ is the ratio of the side/top entering muons given by the muon generator. For Daya Bay near site, we have $r_\mu = 1.2 \text{ Hz/m}^2$ [4], $A = 22 \times 22 \text{ m}^2$, and $\frac{N_{\text{side}}}{N_{\text{top}}} = 1.16$, so $R_\mu = 1.25 \text{ kHz}$.

It is known that neutrons generated inside the rock will lose its energy and initial direction quickly when being transported through the rock. Therefore it is conceivable that one can ignore the neutrons created beyond certain minimum rock thickness. The GEANT4 benchmark program described in [5] was used to study this. Muons with fixed energy are generated along z axis, which strike a large piece of rock ($40 \text{ m} \times 40 \text{ m}$ cross section) with varying thickness. Spallation neutrons are generated by the GEANT4 internal physics

[‡]The prompt visible energy from the neutrons arises from the (quenched) scintillation energy from the slow protons, and its rough relation to the actual KE of the neutron is determined via a separate simulation.

processes described in [5]. Neutrons emerging from the back of the rock with >1 MeV energy are counted. In Fig. 5, the neutron yield as a function of the rock thickness are plotted for several different incident muon energies. One sees that the neutron yield is fairly constant for rock thickness ≥ 1 m. On the other hand, as elaborated in [8], the neutron energy spectrum for thinner rock is harder, which would give a more conservative estimate of the background. Therefore, as mentioned in Sec. 2, we chose to “paint” muons on a box which encloses at least 1 m of rock in the first step.

One should note a few caveats in the above procedure. First, the neutron production in the first step assumes that the neutrons are originated from the muon track. In Fig. 6, the lateral distance of the neutrons (primary and secondary) created by a 200 GeV muon inside liquid scintillator is plotted, based on the GEANT4 benchmark data described in [5]. Therefore, the “along-the-track” approximation for the neutrons is good. Second, as emphasized in [6], the neutron production yield in Eqn. 3 includes *both* primaries and

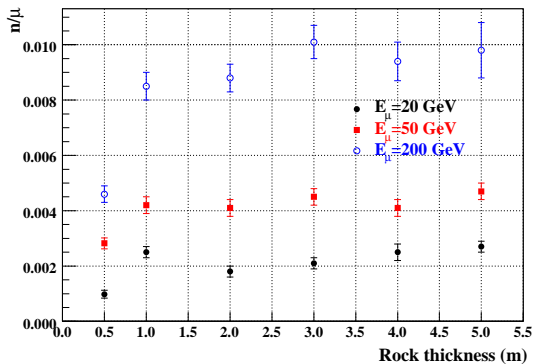


Figure 5: *The neutron production yield vs rock thickness for incident muons of 20, 50, and 200 GeV.*

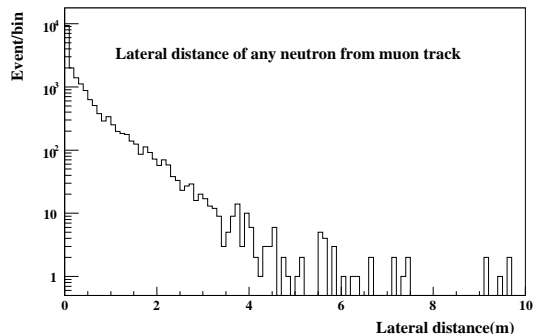


Figure 6: *Lateral distance of neutrons (from the muon track) produced by a 200 GeV muon in liquid scintillator. Data from [5].*

secondaries. Since additional neutrons will be generated during the neutron transport in the second step, some double counting is unavoidable. Third, the contribution from the soft neutrons (less than 100 MeV) could be non-negligible due to their large population. A future improved simulation should make a flat sampling of E_n at the production point from 1 to 2000 MeV and incorporate $\frac{dN}{dE_n}$ into the event weight, rather than making an importance sampling of $\frac{dN}{dE_n}$.

An important uncertainty of this study arises from the GEANT4 treatment to the neutron transport. We cross-checked the GEANT4 neutron attenuation against the MCNPX simulation in [8]. To start with an identical setup, we first obtained a neutron energy spectrum at the far hall by convoluting the muon energy spectrum with the spallation neutron spectrum. These neutrons are then transported through a slab of rock, followed by a slab of water. In Fig. 7, the neutron energy spectra at the production point, after 1 m of rock, and then after 0.5 m of water are plotted. Qualitatively, the softening of the neutron energy spectrum after the rock and water is in agreement with the MCNPX simulation in [8], although the rock neutron spectrum in this work appears to be softer. Based on the same neutron production spectrum, we also studied the gross attenuation coefficient of the neutron through a slab rock with varying thickness. A 1 MeV cut was made on the emerging neutron energy to remove the soft neutrons. The results are shown in Fig. 8 (black circles). Also overlaid (red open squares) is the attenuation of neutrons after 1 m of rock then a slab of water with varying thickness. The resulting attenuation coefficients for the rock and water are 1.7/m and 0.85/m, respectively, which is appreciably less than those in [8]. For a water shield of 2.5 m, this would lead to a factor of 2 difference in neutron rate. The cause of this discrepancy is under investigation.

4 Measurement of the Fast Neutron Background

The spallation neutrons that make into the antineutrino detectors were analyzed in combination with the muon system. Neutrons can be sorted either by their parent muon trajectories, or by their (spallation)

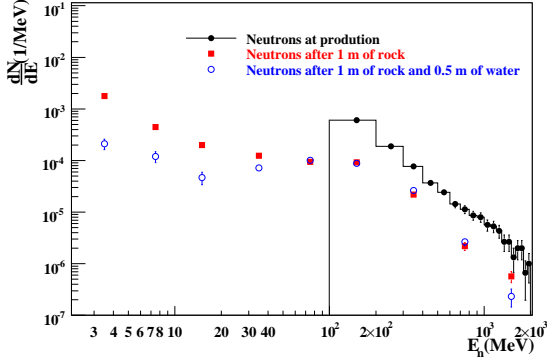


Figure 7: Spallation neutron energy spectrum (far hall) at the production point (black), after 1 m of rock (red), and after 1 m of rock and 0.5 m of water (blue).

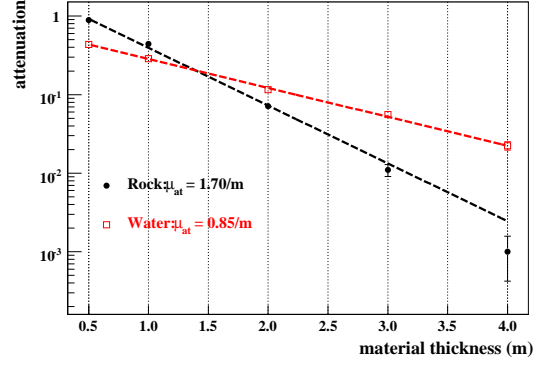


Figure 8: The attenuation of neutron after passing through rock (black) with varying thickness, or 1 m of rock then a slab of water (red) with varying thickness.

production points. For clarity, let us distinguish these two as type I or type II neutrons:

- rock neutrons I – neutrons whose parent muons do not intercept with the water pool;
- water neutrons I – neutrons whose parent muons hit the water pool, but do not make into the AD (AD = scintillator + Gd-loaded scintillator volume but not mineral oil)
- AD neutrons I – neutrons whose parent muons hit the AD;
- rock neutrons II – neutrons which are produced in the rock;
- water neutrons II – neutrons which are produced in the water;
- AD neutrons II – neutrons which are produced in the AD.

In Fig. 9, the energy spectra of these types of fast neutrons entering the target volume are plotted. The peak

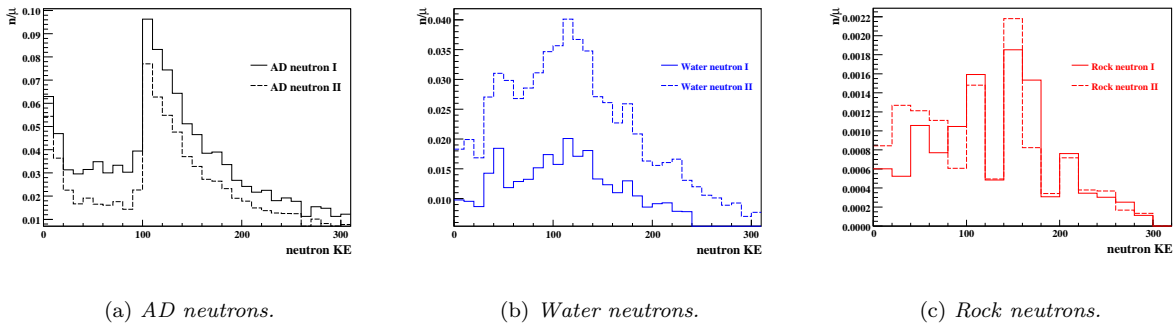


Figure 9: The KE spectra for AD (a), water (b), and rock (c) fast neutrons. Types I and II are represented by the solid and dashed histograms in each figure, respectively.

structure in each figure is due to the 100 MeV cutoff when we sampled the neutron energy at the production. One observes that types I and II spectra for a given media are very similar. Furthermore, the AD spectrum is harder than the other two, which is expected. Due to limited statistics, one can not make a definite statement comparing the water and rock neutron spectra. However, the means of the two distributions from 4 to 2000 MeV are ~ 185 MeV (water) and ~ 145 MeV (rock), which suggests that the rock spectrum is

softer. This is also expected, since the rock neutrons have to go through the entire water thickness, whereas it is less so for the water neutrons. Quantitative studies with higher statistics is needed to further clarify the situation.

Just for future reference, the neutron multiplicity in the target is plotted Fig. 10 for all three type I events; $\sim 30\%$ of the time there are more than one neutrons. In Table 1, the fast neutron rates (see Eqn. 6) at the

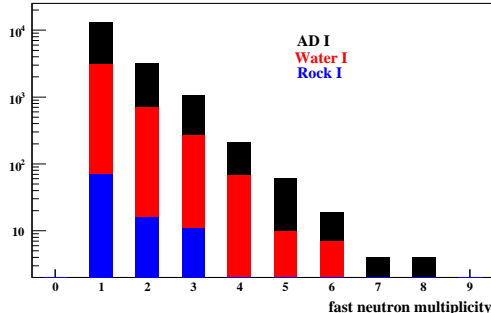


Figure 10: *Fast neutron multiplicity for three different type I events.*

Daya Bay near site for different types of neutrons are summarized. To examine the background rejection ability of the muon system, we also tabulate, for each type of neutrons, the efficiency of the following four veto combinations for tagging their parent muons: (1) “water pool only”: muon track length in water $l_{\mu, \text{water}} > 0.2$ m; (2) “RPC only”: muon crosses RPC; (3) “RPC and no water pool”: muon crosses RPC, and $l_{\mu, \text{water}} < 0.2$ m; (4) “RPC or water pool”: muon either crosses RPC, or with $l_{\mu, \text{water}} > 0.2$ m. The fast

Type	Rate (1/day/module)	tagging efficiency			
		water pool only	RPC only	RPC & no water pool	RPC or water pool
AD I	217	100%	63%	0	100%
Water I	38	99.95%	60%	0	99.95%
Rock I	1.2	0	35%	35%	35%
AD II	180	100%	65%	0	100%
Water II	76	99.75%	60%	0.12%	99.87
Rock II	1.7	25%	42%	23%	48%

Table 1: *Summary table for the fast neutron background rates, and the tagging efficiency of various combination of the veto systems. See text for details.*

neutron rates were calculated by integrating the energy spectra from 4 MeV to 20 MeV, whereas the tagging efficiency is computed by taking the full spectra for better statistics. The fast neutrons rate, as compared to those in the Table 3.5 in [9], are roughly a factor of two too high. It could be due to the treatment of neutron transport in GEANT4, as discussed at the end of Sec. 3. Nevertheless, we note that the main purpose of this work is to study our ability to measure fast neutron background using the veto system, rather than to get absolute rates. Therefore the principle conclusions in this study will not be affected.

Let us make a few observations from Table 1. First, as expected, the water pool efficiency for AD type of neutrons are 100%. Second, the RPC efficiency for tagging the water neutrons is very similar to what we obtained in Sec. 2 for muons. Third, the water pool tagging efficiency for water neutrons is higher than the its overall tagging efficiency for the muons ($\sim 99\%$, see Sec. 2). The reason for this is that muons with short track length in water have less probability to produce water neutrons, effectively leading to an enhancement in the tagging of this type of background. Fourth, the RPC can tag about 1/3 of the rock neutrons, with just 1 m overlap with the rock (Fig. 1). This by itself is already good news. As argued in [2], 1/3 of rock neutron tagging will give us enough statistics to directly measure the rock neutron signals on top of the

accidentals. In Fig. 11, the muon hit locations in (x,y) plane on the RPC are plotted for these tagged rock neutron events. One can see that a large fraction of them are located at a rim with a width about 2 m from the edge of the pool into the rock. This observation has interesting implications. Since we now have better tagging efficiency for the water neutrons than that was originally assumed, it is less crucial to have the RPC to cover the entire top of the pool. Besides, the top center part of the RPC do not help tagging the rock neutrons anyway. It is perhaps useful to extend the RPC further more into the rock to get an even large sample of the rock neutrons. This point requires further validation in simulation.

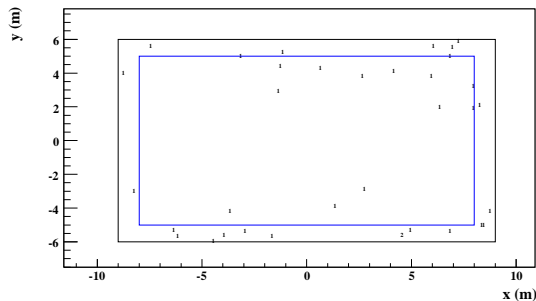


Figure 11: *The muon hit position in (x,y) for the RPC-tagged rock neutron I samples. The black and blue boxes indicate the edge of the RPC and the water pool.*

5 Conclusion

A GEANT4 simulation of the muon system with a water pool and a RPC top has been made for the cosmic muons, as well as for muon-induced neutron background. The principle conclusions of this study are:

- A The inefficiencies of the two muon systems are uncorrelated;
- B The energy spectra for rock and water neutrons are likely different;
- C The water pool efficiency for water neutrons is significantly higher than its efficiency for muons;
- D The current RPC setup can tag $\sim 1/3$ of the rock neutron background.

Conclusion A will allow us to use Laur’s method in [1] to determine the residual “taggable” background, and conclusion D emphasizes the importance of RPC in measuring the “untaggable” rock neutrons.

6 Acknowledgments

I highly appreciate the help and suggestions from Kelly Jordan, David Jaffe, and Laur Littenberg in this study.

References

- [1] L. Littenberg, *Measurement of the Fast Neutron Background*, Daya Bay DocDB #492
- [2] R. D. McKeown, *Fast Neutron Background*, Daya Bay DocDB #550
- [3] J. Liu, *Simulation of the Water Pool Muon Veto System*, Daya Bay DocDB #392
- [4] M. Guan, et al., *Muon simulation at the Daya Bay site*, Daya Bay DocDB #318
- [5] J. Liu, *Geant 4 validation: muon-induced spallation neutrons*, Daya Bay DocDB #582

- [6] Y.-F. Wang, et. al., Phys. Rev. D 64, 013012
- [7] H. M. Araujo, et. al., Nucl. Instrum. Meth. A545, 398
- [8] K. Jordan, K. B. Luk, *Spallation Neutron Production and Attenuation in the Daya Bay Detector Halls*, Daya Bay DocDB #447
- [9] Daya Bay Physics Proposal.